Design and Crystal Structures of Protein Kinase B-Selective Inhibitors in Complex with Protein Kinase A and Mutants

Christine B. Breitenlechner,[‡] Walter-Gunar Friebe,[†] Emmanuel Brunet,[†] Guido Werner,[†] Klaus Graul,[†] Ulrike Thomas,[†] Klaus-Peter Künkele,[†] Wolfgang Schäfer,[†] Michael Gassel,[§] Dirk Bossemeyer,[§] Robert Huber,[‡] Richard A. Engh,[†,‡] and Birgit Masjost[†,*]

Abteilung Strukturforschung, Max-Planck-Institut fuer Biochemie, 82152 Martinsried, Germany, Department of Medicinal Chemistry, Roche Diagnostics GmbH, 82372 Penzberg, Germany, and Department for Pathochemistry, German Cancer Research Center, 69120 Heidelberg, Germany

Received April 21, 2004

Protein kinase B (PKB)-selective inhibitors were designed, synthesized, and cocrystallized using the AGC kinase family protein kinase A (PKA, often called cAMP-dependent protein kinase); PKA has been used as a surrogate for other members of this family and indeed for protein kinases in general. The high homology between PKA and PKB includes very similar ATP binding sites and hence similar binding pockets for inhibitors, with only few amino acids that differ between the two kinases. A series of these sites were mutated in PKA in order to improve the surrogate model for a design of PKB-selective inhibitors. Namely, the PKA to PKB exchanges F187L and Q84E enable the design of the selective inhibitors described herein which mimic ATP but extend further into a site not occupied by ATP. In this pocket, selectivity over PKA can be achieved by the introduction of bulkier substituents. Analysis of the cocrystal structures and binding studies were performed to rationalize the selectivity and improve the design.

Introduction

Kinases are key players in cellular signal transduction pathways. They convey signals which lead to cell growth, proliferation, and apoptosis. Disregulation can cause serious diseases such as cancer. Therefore, kinases have become important targets in pharmaceutical research.[1]

PKB is located downstream in the PI-3 kinase pathway[2,3] and phosphorylates a growing list of substrates involved in several other pathways promoting cell survival and inhibition of apoptosis, as has been shown recently.[4−8] Constitutive activation and overexpression of protein kinase B (PKB/Akt) is found in human prostate, breast, and ovarian carcinomas.[9−11]

It is known that ATP competitive inhibitors are highly potent and efficient inhibitors of kinases. On the other hand, most inhibitors of this kind suffer from a lack of selectivity due to the high conservation of the ATP pocket across the kinases.

PKA was the first kinase to be crystallized, and its structure was solved in 1991 as a binary complex with a peptide inhibitor.[12] Since then the crystal structures of PKA complexed with various substrates and inhibitors[13−19] have been solved and reviewed.[20−22]

PKA has been used as a surrogate kinase for PKB,[15] because PKA and PKB are highly homologous proteins with a sequence identity of 47% in the catalytic kinase domain. Moreover, active site mutants of PKA mimicking PKB were made to improve the surrogate and to obtain information about the contribution of individual amino acid residues to observed binding data.[23] Depending on definitions, there are three to seven amino acid exchanges between PKA (α isoform) and PKB (α and β isoform) in the ATP binding site. Four and five of them have been implemented in the PKAB4 and PKAB5 mutants, respectively. Crystal structures of PKB (Akt2) have been published recently, verifying our surrogate approach.[24−26]

Starting from a class of novel azepane derivatives[13] of the natural product kinase inhibitor (−)-balanol, new compounds have been synthesized to address selectivity issues. They bear larger substituents, chosen to exploit a binding site in PKB which is narrower in PKA. This region lies outside the ATP-binding pocket and is not occupied by the previously reported inhibitors.

Binding studies, cocrystallization and structure determination of these new inhibitors with PKA and PKAB4/5 were performed to analyze the binding properties of these inhibitors for the design of selective inhibitors of PKB versus PKA.

Results and Discussion

Overall Structures. The PKB inhibitors shown in Figure 1 have been cocrystallized with PKA and in some cases additionally with the 4- and 5-fold PKA mutants PKAB4 and PKAB5, with active site mutations V123A, L173M, Q84E, F187L, and in case of PKAB5 additionally Q181K. All inhibitors were cocrystallized under equal conditions with PKI(5−24), MEGA-8, and PKA or PKAB mutants. All crystals belong to the orthorhombic space group with one molecule per asymmetric unit, although differing packing arrangements are observed.

An overlay of the Cα traces of all crystal structures is shown in Figure 2a. All inhibitors bind to the ATP pocket, the cleft between the small N-terminal lobe and larger C-terminal lobe. Only the complex with inhibitor **5** shows a more open conformation. A close-up view of the binding-site shows a good fit for the overlay of all inhibitors in the adenine and ribose pocket, but the benzophenone moieties with their substituents occupy

* To whom correspondence should be addressed. E-mail: birgit.masjost@roche.com. Phone: +49(0)8856/604749. Fax +49(0)-8856/604445.
‡ Max-Planck-Institut, Martinsried.
† Roche Diagnostics GmbH, Penzberg.
§ German Cancer Research Center, Heidelberg.

10.1021/jm049701n CCC: $30.25
Published on Web 12/16/2004

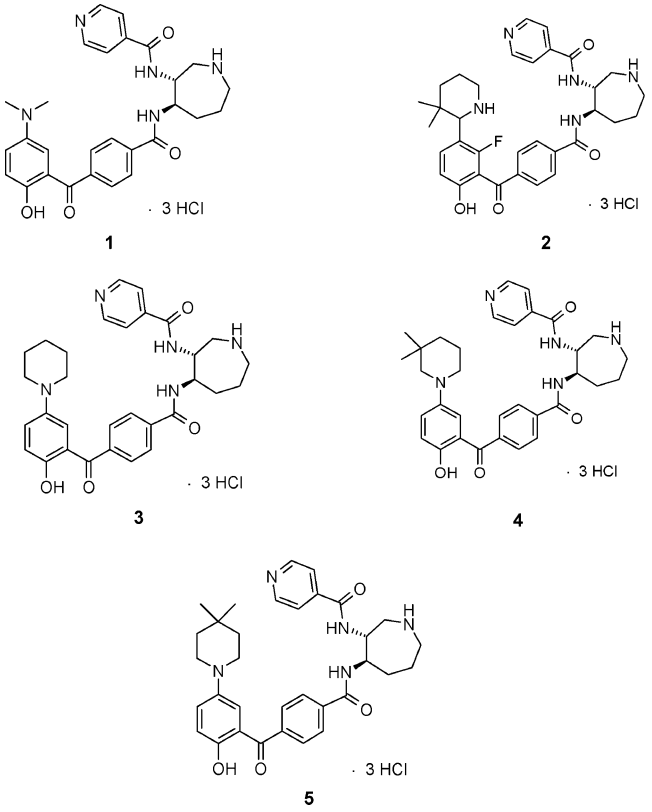

Figure 1. Chemical structures of the inhibitors **1**−**5**.

markedly differing positions. Induced fit movements of the flexible glycine loop can be observed (Figure 2b).

Binding of Inhibitor 1 to PKA and PKAB5 as Surrogate for PKB. Validation of PKAB5 as Surrogate for PKB. Inhibitor **1** is a nanomolar inhibitor of PKB (IC_{50} = 23 nM) and PKA (IC_{50} = 30 nM) (Table 1). Comparison of the crystal structures of **1** in a complex with PKA and PKAB5 (Figure 3) shows a high similarity (rmsd 0.2588 Å) when Cα atoms are fitted. Differences in the active site between the two structures arise from the orientations of the side chains of the amino acids that are mutated in PKAB5. The mutations are clearly defined in the electron density. However, they do not cause meaningful conformational changes or binding interactions in the binding of inhibitor **1** to the active site of the protein. Compared to the recently published PKB structure,[24] the side chains of the mutated amino acids in the crystal structure of **1** with PKAB5 adopt an equivalent rotamer conformation and spatial positions to within accuracies relevant for modeling. Therefore, the PKAB5 mutant is a suitable surrogate for PKB, and cocrystal structures of inhibitors such as **1** with PKAB5 are valuable for the design of inhibitors with PKB/PKA selectivity.

Detailed analyses of inhibitor binding to PKA for ATP competitive inhibitors such as the balanol-derived type inhibitor **1** have been published previously;[13] essentially the same pockets are occupied in all of these structures. Three pockets can be defined as follows: (1) The pyridine and amide occupy the adenine pocket, here referred to as "pyridine pocket". (2) The azepane and second amide stretch across the ribose subsite, here referred to as the "azepane pocket". (3) A large "benzophenone pocket", mostly unoccupied by ATP in the active enzyme, holds the rest of the inhibitor. It is made up of residues from the tip of the glycine loop (S53 and F54), from helix C (L82, Q84, H87, and T88), and from the activation loop (F187).

Three mutations surround the pyridine pocket: L173M, V123A, and Q181K. The charge introduced by the Q181K exchange is too distant from the ligand for strong electrostatic interactions. This mutation was introduced because Q181 can occupy the pyridine pocket in combination with the mutations L173M and V123A. ATP or other ligands force it back into its original position at an energy cost which distorts the apparent binding constants.[23] The L173M mutation has interesting effects on the inhibitor binding. As the sulfur of the methionine side chain is located underneath the inhibitor, interactions with the aromatic system of pyridine turn it out of plane by approximately 10°. This has been observed in all PKAB structures with that inhibitor class solved up to date. The remaining two mutations are adjacent to the benzophenone pocket (Figure 3). Especially the F187L mutation renders the pocket larger than the corresponding pocket of PKA. Thus bulkier substituents might fit selectively into this pocket in PKB but not in PKA. Furthermore, the Q84E exchange is located at a distance to the bound inhibitor near enough for significant electrostatic interactions. In the design of potentially selective inhibitors of PKB (versus PKA) we focused on the exploitation of the exchanges F187L and Q84E.

Design and Binding of Inhibitor 2. In a first approach, inhibitor **2** was designed and synthesized in order to address selectivity issues. The design of this compound was performed on the basis of the cocrystal structure of **1** in PKA with the following considerations: (a) the dimethylamino group of **1** and the two nonconservative mutations Q84E and F187L form a triangle perpendicular to the ring bearing the dimethylamino group. Typically, such a geometry may be achieved by attaching a ring system which contains bulky substituents in the ortho position. (b) A basic group should be attached that could lead to a stronger interaction with glutamate as compared to glutamine. (c) The distances between the attachment point and the two mutations suggest the use of a medium sized ring. Various aromatic and alicyclic five- and six-membered ring systems bearing bulky substituents on one side and basic groups on the opposite side were constructed and docked into PKA and the double mutant Q84E/ F187L. Finally, it turned out that the bulkiness of a dimethylpiperidine should prevent good binding to PKA, because of steric hindrance from the PKA-specific phenylalanine F187. However, it should still bind to PKB, with its larger benzophenone pocket, due to leucine in the equivalent position. At the same time, the "ortho" methyl groups should force the piperidine ring into a geometry perpendicular to the adjacent phenyl group. As a consequence, the amine of the piperidine is oriented exactly against position 84 and could thus make an efficient interaction with the side chain carboxylate of E84 as in the mutants and PKB. Docking studies showed that compound **2** fits nicely into the modeled mutant, but not at all into PKA.

The IC_{50} value for binding of inhibitor **2** to PKA was 2.4 μM as compared to IC_{50}(PKB) = 750 nM (Table 1). Binding constants measured by ITC which can be compared directly are K_D(PKA) = 3.3 μM, K_D(PKAB3)

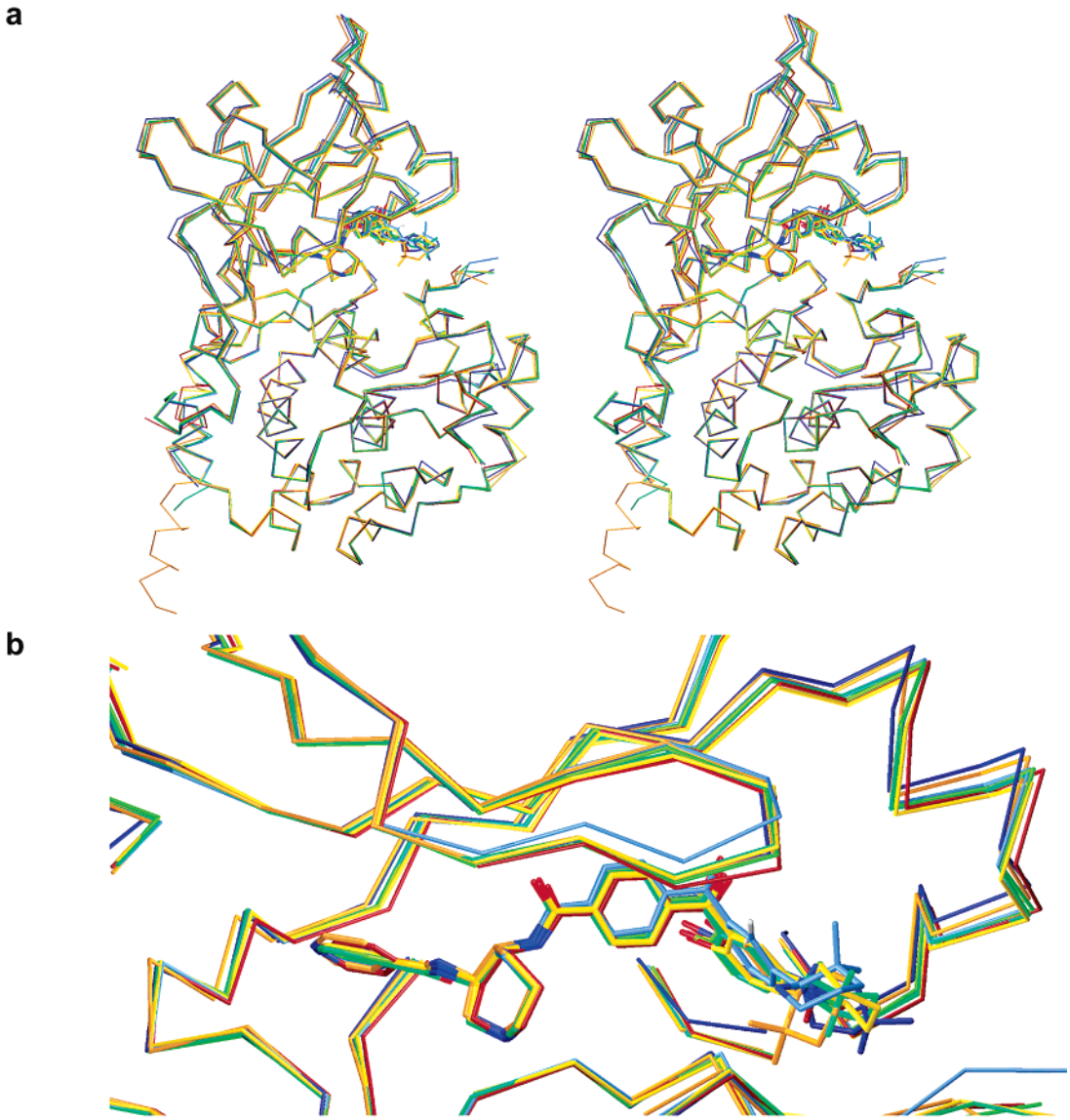

Figure 2. Overlay of all cocrystal structures of the inhibitors **1**−**5** with PKA or PKAB mutants and the pseudosubstrate inhibitor peptide PKI(5−24). (a) Overlay of the Cα traces. The inhibitors are ATP competitive and bind to the ATP pocket, the cleft between the small N-lobe and larger C-lobe. (b) Close-up view of the inhibitors in the ATP binding pocket.

Table 1. IC_{50} Values (nM) and Standard Deviations Measured for Binding of Inhibitors to PKA and PKB

inhibitor	IC_{50} (PKA)	IC_{50} (PKB)
1	30 ± 28	23 ± 7
2	2400 ± 1800	750 ± 340
3	400 ± 160	20 ± 6
4	1900 ± 1000	20 ± 18
5	1700 ± 600	40 ± 6

= 3.7 μM, and K_D(PKAB5) = 260 nM (Table 2), i.e., inhibitor **2** displays a selectivity for PKAB5 over PKA and PKAB3 by a factor of 12. The cocrystal structure of the complex of inhibitor **2** with PKA shows that the positions of pyridine and azepane are nearly unchanged compared to inhibitor **1**, whereas the benzophenone and piperidine substituents differ (Figure 2b, 4). The H-bond of the benzophenone substituent OH to K72 as seen in the crystal complex of inhibitor **1** cannot be formed anymore (in a distance of 3.7 Å) and also its interaction to E91 is weak. The hydroxyl group is in a distance of 4.3 Å from the E91 carboxylate group which is usually in a tight interaction in all other structures. However, a water molecule bridges the inhibitor and E91. Moreover, inhibitor **2** induces a shift in the position of the glycine loop caused by the piperidine ring that is rotated with the methyl groups oriented toward S53 and Q84 as a consequence of the steric clash between the methyl groups and the phenyl group of F187. Consequently, there are strong repulsive van der Waals interactions between the S53 hydroxyl group from the tip of the glycine loop and the methyl substituents of the piperidine ring.

This unfavorable binding conformation explains the lower binding affinity of inhibitor **2** to PKA and PKAB3 compared to compound **1**. Only the PKAB5 mutant shows good binding. The kinetic data demonstrate that the additional two mutations in the benzophenone pocket are important for the affinity while the three mutations in the pyridine pocket do not have a significant effect.

This inhibitor was also crystallized with the PKAB4 mutant (including both amino acid exchanges in the benzophenone pocket), and the structure reveals that

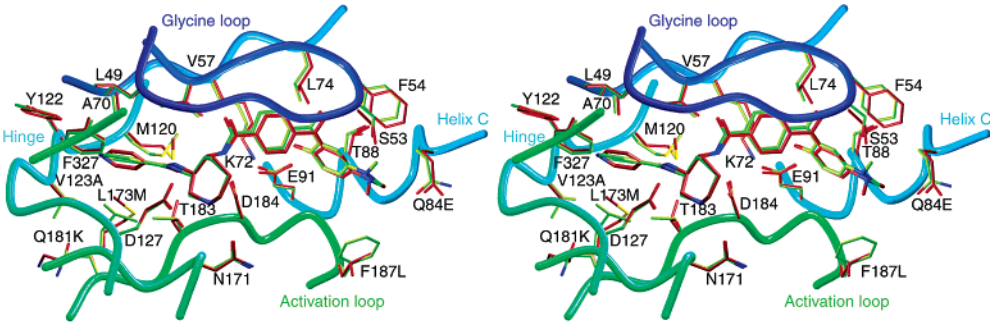

Figure 3. Overlay of the cocrystal structures of inhibitor **1** with PKA (green) and PKAB5 (red) mutant. The inhibitor binding site is depicted with all amino acids in van der Waals contacts with the ligand including the five mutations. The mutations do not cause conformational changes or changes of binding interactions of inhibitor **1** to the active sites of the proteins.

Table 2. K_D Values and Standard Deviations Measured with ITC for Binding of Inhibitors to PKA and PKAB Mutants

inhibitor	K_D (PKA) [nM]	K_D (PKAB3) [nM]	K_D (PKAB5) [nM]
1	34 ± 10	41 ± 9	17 ± 6
2	3400 ± 1400	3770 ± 1230	260 ± 100
3	48 ± 20	193 ± 72	9 ± 7
4	150 ± 63	77 ± 27	8 ± 5

the glycine loop is in a "normal" position. This is due to the F187L mutation being less bulky and leaving more space for the inhibitor in the pocket. Thus, the glycine loop is not displaced.

The position of the benzophenone substituent differs in both structures of inhibitor **2**. Both methyl substituents of the piperidine make use of the additional space in the binding pocket. They are oriented toward L187 and G186. This conformation is rotated nearly 180° compared to the structure of the complex with PKA (Figure 4). Thus, the piperidine nitrogen is oriented toward E84 and forms an H-bond with its side chain as predicted by molecular modeling. However, the side chain has to rearrange to make this hydrogen bond compared to the structure of inhibitor **1** in the PKAB5 mutant. Moreover, the conformation of inhibitor **2** as it is bound to the PKAB4 mutant shows unfavorable repulsive van der Waals contacts between the fluorine substituent of the benzophenone and the piperidine nitrogen and one methyl group. The adoption of this unfavorable conformation of the inhibitor and the missing tight H-bond of the benzophenone OH with the enzyme residue E91 might explain its 10 times lower binding affinity for PKB and PKAB5 as compared to inhibitor **1.**

Binding of Inhibitor 3. Based upon the knowledge and experience gained from the crystal structures of inhibitors **1** and **2**, inhibitors **3**, **4**, and **5** were designed to further explore the exploitation of the differences in the amino acids 187 and 84 between PKA and PKB to obtain selective inhibitors for PKB. The IC_{50} (PKB) values of inhibitors **3**, **4**, and **5** are in the low nanomolar region (Table 1). The IC_{50} (PKA) values are higher by a factor of 20 for inhibitor **3**, by a factor of 95 for inhibitor **4**, and by a factor of 43 for inhibitor **5**. Clearly, they are all selective inhibitors of PKB versus PKA. The cocrystal structures with PKA clarify the binding modes (Figure 5).

Analysis of inhibitor **3** cocrystallized with PKA (Figure 5a) reveals minor changes at the glycine loop, F187, and PKI(5−24) as compared to inhibitor **1**: the glycine loop moves up, but there are still steric conflicts between the benzophenone and F54 from the tip of the glycine loop. As a consequence, the usually tight H-bond between the inhibitor and E91 is apparently weakened, but still within a hydrogen bonding distance (3.0 Å). It can be rationalized that these changes cause the lower affinity of inhibitor **3** for PKA compared to inhibitor **1** by a factor of 2 (K_D) or 10 (IC_{50} values). Data from ITC experiments show that the K_D(PKA) = 48 nM and K_D(PKAB3) = 190 nM is 5 and 20 times respectively higher than the K_D(PKAB5) = 9 nM.

Figure 5 shows the inhibitors **3**, **4**, and **5** with their omit $F_o - F_c$ electron density maps. The piperidine ring of inhibitor **3** is probably flexible and can adopt different conformations because there is only a weak difference electron density for the piperidine compared to the rest of the molecule.

Binding of Inhibitor 4. Inhibitor **4** is the most selective for PKB versus PKA. It has an approximately 100 times higher affinity judged from IC_{50} values. In the crystal structure of **4** with PKA (Figure 5b) there are no obvious changes in the conformation of the protein compared to the structure of **3**. However, the piperidine moiety of inhibitor **4** adopts an envelope conformation because of sterical hindrance caused by the two methyl groups to avoid a steric clash with F187. This is energetically unfavorable and explains the low affinity of the inhibitor for PKA (IC_{50} = 1.9 μM). Again, ITC experiments showed binding constants for PKA and PKAB3 in the high nM range (150 nM and 77 nM, respectively), while the binding constant for PKAB5 is as low as 8 nM. This factor of 20 is thus shown to be the effect of the two additional mutations in the benzophenone pocket, most probably due to the steric effect of the F187L amino acid exchange rather than the Q84E mutation.

Binding of Inhibitor 5. Inhibitor **5** is selective for PKB versus PKA as well. Its low binding affinity for PKA (IC_{50} = 1.7 μM) can be interpreted from its crystal structure in complex with PKA which was solved at 1.68 Å resolution. The structure was refined to a final R-factor of 20.0% (R-free 23.5%). The inhibitor binds to PKA in a similar way as inhibitor **1**, but extends further into the pocket. This leads to several conformational changes of the PKA protein: namely, the side chain of F187 is shifted to avoid a steric clash with the bulky dimethyl substituents of the inhibitor. As a consequence, C199 in the activation loop also changes its side chain orientation and additionally, the main chain atoms of the activation loop are shifted away from helix C. pThr197 is dislocated by about 1 Å in a concerted

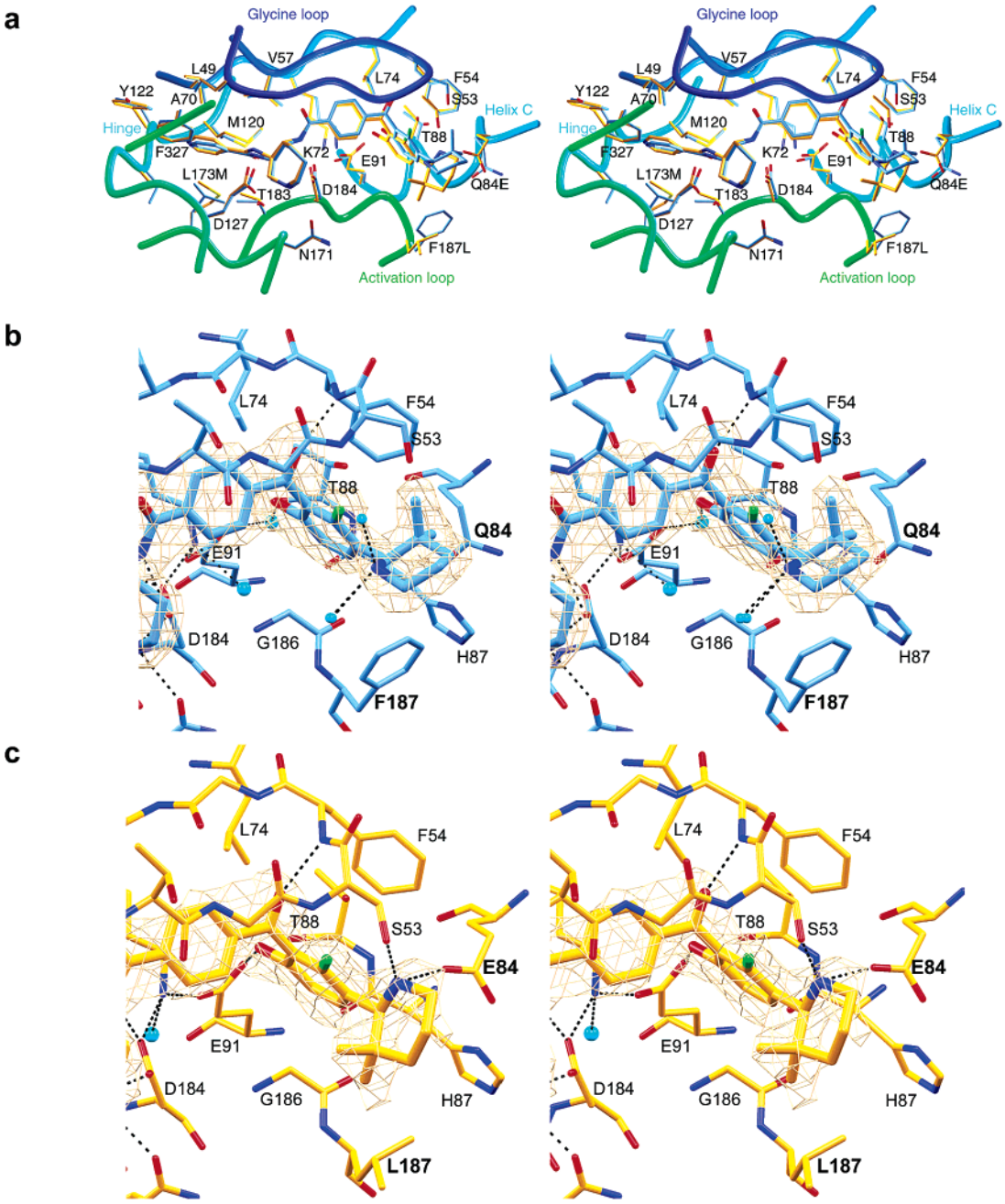

Figure 4. Binding of inhibitor **2** to PKA and the PKAB4 mutant. (a) The overlay of the cocrystal structures of inhibitor **2** with PKA (blue) and PKAB4 (yellow) shows that the positions of pyridine and azepane are nearly unchanged, whereas the benzophenone and piperidine substituents differ. The substituents are rotated nearly 180°. (b) Cocrystal structure with PKA. The benzophenone part of inhibitor **2** is shown with an omit $F_o - F_c$ electron density map contoured at 2σ. H-bonds are indicated by dotted lines. (c) Cocrystal structure with PKAB4. The benzophenone part of inhibitor **2** is shown with an omit $F_o - F_c$ electron density map contoured at 2σ. H-bonds are indicated by dotted lines.

movement with R165 and K189. In contrast, the salt bridge between pT197 and H87 cannot be formed anymore, as Helix C is shifted away from pT197 at the same time (Figure 5c). Moreover, the enzyme is a bit more open than in the other structures. The cost in energy which is needed to induce these conformational changes in PKA upon binding of the inhibitor **5** explains its low binding affinity. Molecular modeling shows that, in the case of PKB or PKAB mutants with F187L, there is more space for the bulky dimethyl substituents on the piperidine because of the smaller amino acid leucine. We can assume that upon binding of inhibitor **5** to PKB no induced fit movement of the activation loop takes place, which explains the nanomolar affinity of inhibitor **5** for PKB.

Conclusions

Inhibitors **3**, **4**, and **5** are nanomolar inhibitors of PKB and selective versus PKA. The crystal structures in complex with PKA show that they all occupy the same binding pockets in PKA. However, the piperidine adopts different conformations upon binding to PKA and/or induces conformational changes in its binding pocket in the protein because of unfavorable steric contacts with the side chain of F187. Molecular modeling shows

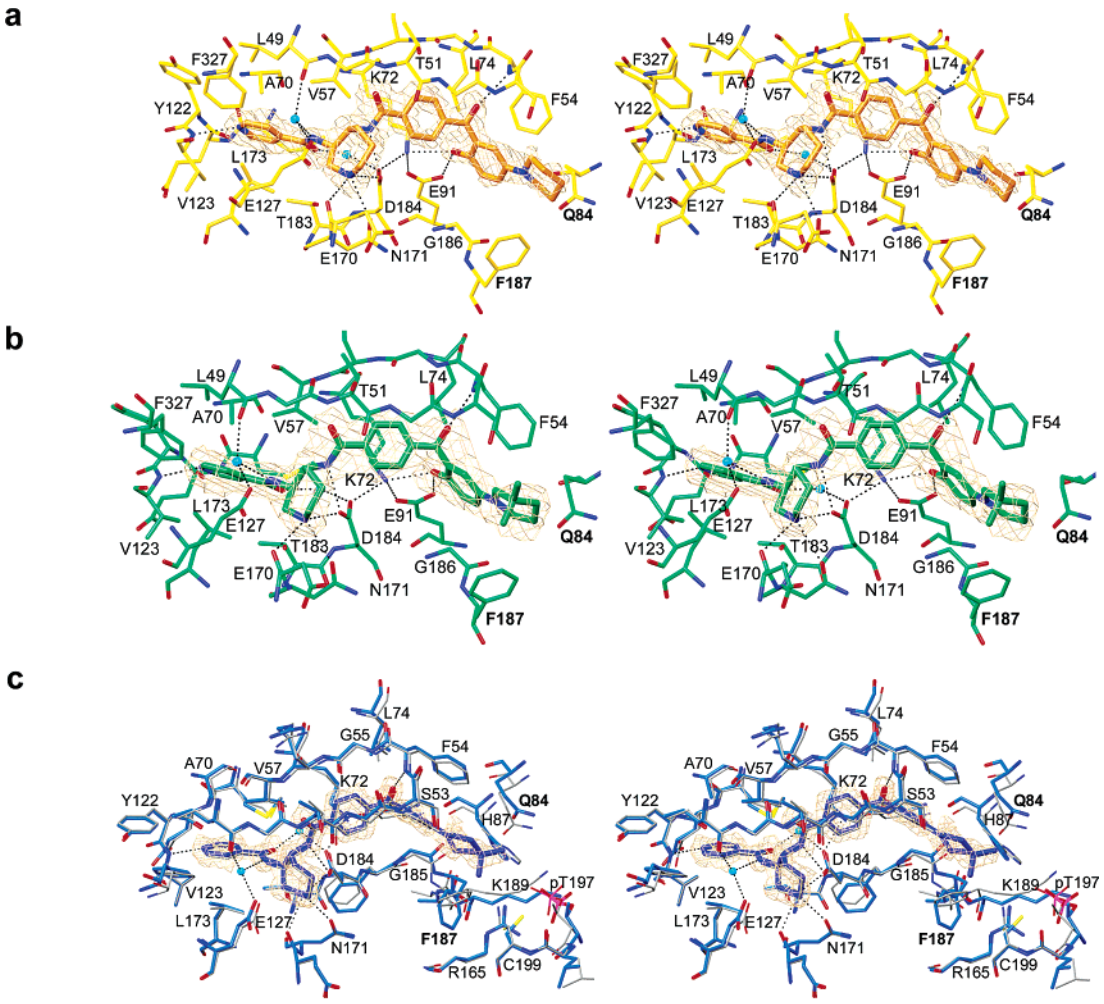

Figure 5. The cocrystal structures of inhibitors **3** (a, yellow), **4** (b, green), and **5** (c, blue) with PKA. All residues involved in van der Waals contacts are shown. The omit $F_o - F_c$ electron density map is contoured at 2σ. H-bonds are indicated by dotted lines. In case of inhibitor **5** (c, blue) the cocrystal structure of inhibitor **1** is superimposed. Neighboring residues of L187 and induced changes in the activation loop are shown.

that these energetically costly conformational changes as well as the unfavorable interactions do not occur in the modeled complexes of the inhibitors bound to PKB due to the expanded space in the F187L mutant which serves as a homology model for PKB.

It has been shown that molecular modeling of inhibitors selective for PKB versus PKA has been successful based on information gained from the crystal structures of the PKAB mutants and homology models.

Still there are more differences in the residues between PKA and PKB in the binding pocket of piperidine and its immediate vicinity which can be used for designing more specific inhibitors. The mutation in Q84E introduces a different electrostatic environment ($RCONH_2$ versus RCOO(H)) which has been rationalized in the design of inhibitor **2**.

The mutations S53T and L82K at the piperidine binding pocket could also be used for the design of PKB/PKA selectivity based on diverse substitution of the piperidines. Currently, these mutations are being implemented in new PKAB mutants that will similarly enable the identification of new mechanisms for selectivity.

Experimental Section

Inhibitor Synthesis. The synthesis of the azepine portion and its coupling to the benzophenone portion of the inhibitors (3*R*,4*R*)-*N*-{4-[4-(5-dimethylamino-2-hydroxybenzoyl)benzoylamino]azepan-3-yl}isonicotinamide hydrochloride (**1**), (3*R*,4*R*)-*N*-(4-{4-[3-(3,3-dimethylpiperidin-2-yl)-2-fluoro-6-hydroxybenzoyl]benzoylamino}azepan-3-yl)isonicotinamide hydrochloride (**2**), (3*R*,4*R*)-*N*-{4-[4-(2-hydroxy-5-piperidin-1-ylbenzoyl)benzoylamino]azepan-3-yl)isonicotinamide hydrochloride (**3**), (3*R*,4*R*)-*N*-(4-{4-[5-(3,3-dimethylpiperidin-1-yl)-2-hydroxybenzoyl]benzoylamino}azepan-3-yl)isonicotinamide hydrochloride (**4**), and (3*R*,4*R*)-*N*-(4-{4-[5-(4,4-dimethylpiperidin-1-yl)-2-hydroxybenzoyl]benzoylamino}azepan-3-yl)isonicotinamide hydrochloride (**5**) (Figure 1) was performed as recently published.[13,27] The benzophenone portions of the molecules were synthesized by the assembly of 4-formylbenzoic acid methyl ester and the respective substitued 4-aminophenol.[28,29] The 4-aminophenols were synthesized as follows: for the synthesis of **1**, 4-dimethylaminophenol was synthesized from 4-methoxyphenylamine by double methylation of the amino functionality with dimethyl sulfate followed by cleavage of the methoxy ether with boron tribromide to give the corresponding phenol.[30] For the synthesis of **2**, 4-(3,3-dimethylpiperidin-2-yl)-3-fluorophenol was synthesized starting from 1-fluoro-3-methoxybenzene by friedel crafts acylation[31] with isobutyric acid anhydride to give 1-(2-fluoro-4-methoxyphenyl)-2-methylpropan-1-one which was then reacted by cyanoethylation[32] to give 5-(2-fluoro-4-methoxyphenyl)-4,4-dimethyl-5-oxopentanenitrile from which the product was obtained by ring closure,[33] hydrogenation, and demethylation. 4-Piperidin-1-ylphenol was synthesized by reaction of 4-methoxyphenylaniline with 1,5-dibromopentane,[34] followed by demethylation. 4-(3,3-Dimethylpiperidin-1-yl)phenol and 4-(4,4-dimethylpiperidin-1-yl)phenol were synthesized starting from 4-methoxyphenylaniline which

Table 3. Data Collection and Refinement Statistics

	PKA/PKAB mutant inhibitor						
	PKA 1	PKAB5 1	PKA 2	PKAB4 2	PKA 3	PKA 4	PKA 5
			Data Collection				
X-ray source/beam line	rotating anode	DESY-BW6	DESY-BW6	DESY-BW6	DESY-BW6	DESY-BW6	SLS-PX
wavelength (Å)	1.54179	1.05	1.05	1.05	1.05	1.05	1.00076
space group	$P2_12_12_1$	$P2_12_12_1$	$P2_12_12_1$	$P2_12_12_1$	$P2_12_12_1$	$P2_12_12_1$	$P2_12_12_1$
cell (a, b, c) (Å)	73.0	61.7	74.1	49	61.4	73.8	70.7
	79.1	78.8	76.8	79	76.0	75.4	73.3
	79.1	78.8	79.5	117	78.7	79.4	78.1
resolution range (Å)	33.1−2.45	16.9−1.64	18.6−2.05	15−2.46	16.4−1.9	17.5−2.47	23.1−1.6[a]
number of unique reflections	17307	46553	29100	17124	29593	16350	50095
completeness (%) [last shell]	98.8 [96.1]	98.1 [94.2]	99.8 [100]	97.4 [87.4]	98.7 [96.8]	98.7 [96.8]	93.2 [100]
I/σ (I) [last shell]	10.0 [3.7]	6.1 [1.3]	7.1 [1.6]	4.8 [1.7]	6.2 [1.5]	3.1 [2.3]	1.6 [2.5]
average redundancy [last shell]	4.3 [3.9]	3.8 [3.7]	5.5 [5.5]	2.7 [3.0]	3.2 [3.1]	4.2 [4.1]	3.6 [3.8]
R_{sym} [last shell]	6.2 [20.8]	9.4 [53.8]	8.1 [44.2]	12.2 [38.6]	9.4 [46.9]	9.3 [33.3]	16.4 [26.2]
			Refinement				
number of atoms in refinement	3040	3328	3200	3078	3245	3100	3421
reflections used	16412	44150	27600	16210	28049	15481	44536*
R-factor/free R-factor (%)	18.9/24.2	16.6/19.8	18.2/23.6	22.2/27.2	18.9/24.9	18.8/25.4	20.0/23.5
free R-value test size (%)	5.0	5.1	5.0	5.1	5.1	5.0	5.1
correlation coefficient $F_o - F_c$ [free]	93.3 [89.9]	96.3 [94.4]	95.5 [92.0]	91.9 [88.7]	94.6 [91.0]	94.6 [91.0]	93.2 [90.4]
			Standard Deviation from Ideal Values				
bond length (Å)	0.019	0.012	0.016	0.015	0.017	0.015	0.014
bond angles (deg)	1.622	1.345	1.503	1.428	1.520	1.496	1.412
			Temperature Factors				
all atoms	27.3	18.1	29.6	33.9	22.9	37.4	16.5

[a] Ice rings omitted only in refinement.

was reacted with 2,2,-dimethylpentanedioic acid and 3,3-dimethylpentanedioic acid, respectively,[35] to generate 1-(4-methoxyphenyl)-4,4-dimethylpiperidine-2,6-dione and 1-(4-methoxyphenyl)-3,3-dimethylpiperidine-2,6-dione. The products were obtained after reduction with lithium aluminum hydride followed by demethylation.

Mutagenesis of PKA. Site-directed mutagenesis was performed using pT7-PKA as template and the Stratagene (La Jolla) QuikChange kit following the manual of the supplier including the design of the corresponding primer pairs and as previously published.[15] All constructs used for protein expression were verified by DNA sequencing. The PKAB4 mutant has amino acid exchanges only within the ATP binding pocket. They are compared to wild-type protein: V123A, L173M, Q84E, and F187L. PKAB5 has additionally the Q181K exchange.

Expression and Purification. Expression vectors pT7-7 and pET28b, both carrying a T7-promoter, were used to express bovine PKA Cα, PKAB4, and PKAB5 in *Escherichia coli* strain BL21 (DE3), respectively. Two positions distinguish bovine (N32, M63) from human PKA (S32, K63). Protein was expressed and purified via affinity chromatography and ion exchange chromatography as described previously.[17,23,36] The identity of the protein samples and the phosphorylation state was confirmed by mass spectrometry.

X-ray Crystallography. Hanging droplets containing 18 mg/mL protein, 25 mM Mes-BisTris pH6.4, 75 mM LiCl, 1.5 mM octanoyl-*N*-methylglucamide (MEGA-8), 1 mM PKI(5−24) were equilibrated at 4 °C against 12 to 18% methanol. Diffraction data of the flash frozen crystals were measured at home with a rotating anode X-ray generator Rigaku R300 or at the synchrotron beamlines BW-6 at the DESY (Hamburg, Germany) and PX at the SLS (Villigen, Switzerland). The data were processed with the program MOSFLM and SCALA. The crystals have the orthorhombic symmetry $P2_12_12_1$; for details see Table 3. The structures were determined by molecular replacement using AMoRe from the CCP4 program package (www.ccp4.ac.uk/main/html).[37,38] As starting model we chose a PKA structure in a closed conformation (unpublished results). Refmac (version 5.1.24) was used for refinement, while MOLOC[39] (www.moloc.ch) was used for graphical evaluation and model building. The structures are depicted in the Figures 1 and 2 with graphics from programs MOLSCRIPT,[40] BOBSCRIPT,[41] and Raster3d.[42] Atomic coordinates have been deposited in the Protein Data Bank with accession numbers 1XH4, 1XH5, 1XH6, 1XH7, 1XH8, 1XH9, 1XHA.

Enzymatic Assays. Enzymatic assays have been carried out as previously described.[13]

Isothermal Titration Calorimetry (ITC). For ITC experiments the protein has been dialyzed in 20 mM HEPES pH 7.5, 10 mM $MgCl_2$, 0.1 mM $CaCl_2$, 50 mM KCl. Measurements were carried out using the VP−ITC instrument from MicroCal. The protein concentration in each experiment was accurately determined and about 20 μM. The ligand (c = 0.5 mM to 1 mM) was titrated to the protein. Experimental data was analyzed using Origin 5.0 software. Results are presented in Table 2.

Molecular Modeling. The design of target molecules was carried out on a Silicon Graphics Octane workstation. The starting geometries for the molecular mechanics studies were constructed with the program MOLOC, from crystallographic data and standard molecular fragments. The proposed inhibitor was minimized separately and docked manually into its expected binding site. The coordinates of PKA were constrained. The inhibitors were minimized inside the enzyme. Energy minimizations were performed in vacuo by MOLOC with the MAB force field. The energy was minimized by conjugate gradients to a final value of the sum of the squares of the components of the gradient of less than the accuracy (0.1 or relative value of 1). For docking studies of mutants of PKA (Q84E, F187L), homology models were created by exchanging and subsequent optimization of the respective side chains.

Sequence Alignment and Homology Model Building. Sequences were aligned using the ClustalW-server from http://www.ebi.ac.uk/clustalw/. Homology models were calculated by the SWISS-MODEL Protein Modeling Server (http://www.expasy.ch/swissmod/SWISS-MODEL.html).

Acknowledgment. We thank Dr. W. von der Saal and Dr. A. Mertens for encouragement and support. We thank Prof. Dr. F. Diederich for consulting and helpful discussions of this work.

Appendix

Abbreviations: PKA, protein kinase A; cAMP dependent protein kinase; PKAB4, mutant of PKA with V123A,

L173M, Q84E, and F187L; PKAB5, mutant of PKA with V123A, L173M, Q84E, Q181K, and F187L; PKB, protein kinase B, Akt.

References

(1) Cohen, P. Protein kinases − the major drug targets of the twenty-first century? *Nat. Rev. Drug Discovery* **2002**, *1*, 309−315.

(2) Vanhaesebroeck, B.; Alessi, D. R. The PI3K−PDK1 connection: more than just a road to PKB. *Biochem. J.* **2000**, *346 Pt 3*, 561−576.

(3) Alessi, D. R.; Cohen, P. Mechanism of activation and function of protein kinase B. *Curr. Opin. Genet. Dev.* **1998**, *8*, 55−62.

(4) Blume-Jensen, P.; Hunter, T. Oncogenic kinase signaling. *Nature* **2001**, *411*, 355−365.

(5) Datta, S. R.; Brunet, A.; Greenberg, M. E. Cellular survival: a play in three Akts. *Genes Dev.* **1999**, *13*, 2905−2927.

(6) Kandel, E. S.; Hay, N. The regulation and activities of the multifunctional serine/threonine kinase Akt/PKB. *Exp. Cell Res.* **1999**, *253*, 210−229.

(7) Testa, J. R.; Bellacosa, A. AKT plays a central role in tumorigenesis. *Proc. Natl. Acad. Sci. U.S.A.* **2001**, *98*, 10983−10985.

(8) Vivanco, I.; Sawyers, C. L. The phosphatidylinositol 3-Kinase AKT pathway in human cancer. *Nat. Rev. Cancer* **2002**, *2*, 489−501.

(9) Thakkar, H.; Chen, X.; Tyan, F.; Gim, S.; Robinson, H.; Lee, C.; Pandey, S. K.; Nwokorie, C.; Onwudiwe, N.; Srivastava, R. K. Pro-survival function of Akt/protein kinase B in prostate cancer cells. Relationship with TRAIL resistance. *J. Biol. Chem.* **2001**, *276*, 38361−38369.

(10) Malik, S. N.; Brattain, M.; Ghosh, P. M.; Troyer, D. A.; Prihoda, T.; Bedolla, R.; Kreisberg, J. I. Immunohistochemical demonstration of phospho-Akt in high Gleason grade prostate cancer. *Clin. Cancer Res.* **2002**, *8*, 1168−1171.

(11) Stal, O.; Perez-Tenorio, G.; Akerberg, L.; Olsson, B.; Nordenskjold, B.; Skoog, L.; Rutqvist, L. E. Akt kinases in breast cancer and the results of adjuvant therapy. *Breast Cancer Res.* **2003**, *5*, R37−44.

(12) Knighton, D. R.; Zheng, J. H.; Teneyck, L. F.; Ashford, V. A.; Xuong, N. H.; Taylor, S. S.; Sowadski, J. M. Crystal-structure of the catalytic subunit of cyclic adenosine-monophosphate dependent protein-kinase. *Science* **1991**, *253*, 407−414.

(13) Breitenlechner, C. B.; Wegge, T.; Berillon, L.; Graul, K.; Marzenell, K.; Friebe, W.-G.; Thomas, U.; Schumacher, R.; Huber, R.; Engh, R. A.; Masjost, B. Structure-based optimization of novel azepane derivatives as PKB inhibitors. *J. Med. Chem.* **2004**, *47*, 1375−1390.

(14) Gassel, M.; Breitenlechner, C. B.; Konig, N.; Huber, R.; Engh, R. A.; Bossemeyer, D. The protein kinase C inhibitor bisindolyl maleimide 2 binds with reversed orientations to different conformations of protein kinase A. *J. Biol. Chem.* **2004**, *279*, 23679−23690.

(15) Breitenlechner, C.; Gassel, M.; Hidaka, H.; Kinzel, V.; Huber, R.; Engh, R. A.; Bossemeyer, D. Protein kinase A in complex with rho-kinase inhibitors Y-27632, fasudil, and H-1152P: Structural basis of selectivity. *Structure* **2003**, *11*, 1595−1607.

(16) Prade, L.; Engh, R. A.; Girod, A.; Kinzel, V.; Huber, R.; Bossemeyer, D. Staurosporine-induced conformational changes of cAMP-dependent protein kinase catalytic subunit explain inhibitory potential. *Structure* **1997**, *5*, 1627−1637.

(17) Engh, R. A.; Girod, A.; Kinzel, V.; Huber, R.; Bossemeyer, D. Crystal structures of catalytic subunit of cAMP-dependent protein kinase in complex with isoquinolinesulfonyl protein kinase inhibitors H7, H8, and H89 − Structural implications for selectivity. *J. Biol. Chem.* **1996**, *271*, 26157−26164.

(18) Narayana, N.; Diller, T. C.; Koide, K.; Bunnage, M. E.; Nicolaou, K. C.; Brunton, L. L.; Xuong, N. H.; Ten Eyck, L. F.; Taylor, S. S. Crystal structure of the potent natural product inhibitor balanol in complex with the catalytic subunit of cAMP-dependent protein kinase. *Biochemistry* **1999**, *38*, 2367−2376.

(19) Akamine, P.; Madhusudan; Brunton, L. L.; Ou, H. D.; Canaves, J. M.; Xuong, N.-h.; Taylor, S. S. Balanol analogues probe specificity determinants and the conformational malleability of the cyclic 3′,5′-adenosine monophosphate-dependent protein kinase catalytic subunit. *Biochemistry* **2004**, *43*, 85−96.

(20) Johnson, D. A.; Akamine, P.; Radzio-Andzelm, E.; Madhusudan; Taylor, S. S. Dynamics of cAMP-dependent protein kinase. *Chem. Rev.* **2001**, *101*, 2243−2270.

(21) Engh, R. A.; Bossemeyer, D. The protein kinase activity modulation sites: Mechanisms for cellular regulation − Targets for therapeutic intervention. *Adv. Enzyme Regul.* **2001**, *41*, 121−149.

(22) Breitenlechner, C.; Engh, R. A.; Huber, R.; Kinzel, V.; Bossemeyer, D.; Gassel, M. The typically disordered N-terminus of PKA can fold as a helix and project the myristoylation site into solution. *Biochemistry* **2004**, *43*, 7743−7749.

(23) Gassel, M.; Breitenlechner, C. B.; Ruger, P.; Jucknischke, U.; Schneider, T.; Huber, R.; Bossemeyer, D.; Engh, R. A. Mutants of protein kinase a that mimic the ATP-binding site of protein kinase B (AKT). *J. Mol. Biol.* **2003**, *329*, 1021−1034.

(24) Yang, J.; Cron, P.; Good, V. M.; Thompson, V.; Hemmings, B. A.; Barford, D. Crystal structure of an activated Akt/protein kinase B ternary complex with GSK3-peptide and AMP−PNP. *Nat. Struct. Biol.* **2002**, *9*, 940−944.

(25) Yang, J.; Cron, P.; Thompson, V.; Good, V. M.; Hess, D.; Hemmings, B. A.; Barford, D. Molecular mechanism for the regulation of protein kinase B/Akt by hydrophobic motif phosphorylation. *Mol. Cell* **2002**, *9*, 1227−1240.

(26) Huang, X.; Begley, M.; Morgenstern, K. A.; Gu, Y.; Rose, P.; Zhao, H. L.; Zhu, X. T. Crystal structure of an inactive Akt2 kinase domain. *Structure* **2003**, *11*, 21−30.

(27) Masjost, B.; Schumacher, R.; Friebe, W.-G. Novel azepane derivatives. PCT Int. Appl. (Roche Diagnostics GmbH, Germany): WO03/076429, 2003.

(28) Barbier, P.; Huber, I.; Schneider, F.; Stadlwieser, J.; Taylor, S. Preparation of 3-amino/hydroxy-4-[4-benzoylphenylcarboxylamino/oxy]azepine and homologue protein kinase inhibitors. Eur. Pat. Appl. (F. Hoffmann-La Roche AG, Switz.). EP663393, 1995; 47 pp.

(29) Barbier, P.; Stadlwieser, J.; Taylor, S. Novel azepanes and their ring homologues for therapy and prophylaxis of protein kinase mediated diseases. PCT Int. Appl. (F. Hoffmann-La Roche Ag, Switz.). WO9702249, 1997; 43 pp.

(30) Jaeger, D. A.; Finley, C. T.; Walter, M. R.; Martin, C. A. Preparation and characterization of base-sensitive destructible surfactants. *J. Org. Chem.* **1986**, *51*, 3956−3959.

(31) Ranu, B. C.; Ghosh, K.; Jana, U. Simple and Improved Procedure for Regioselective Acylation of Aromatic Ethers with Carboxylic Acids on the Solid Surface of Alumina in the Presence of Trifluoroacetic Anhydride. *J. Org. Chem.* **1996**, *61*, 9546−9547.

(32) McKinney, L. L.; Uhing, E. H.; Setzkorn, E. A.; Cowan, J. C. Cyanoethylation of a-amino acids. I. Monocyanoethyl derivatives. *J. Am. Chem. Soc.* **1950**, *72*, 2599−2603.

(33) Albertson, N. F. Piperidine and azabicyclo compounds. I. Via Michael condensations. *J. Am. Chem. Soc.* **1950**, *72*, 2594−2599.

(34) Periasamy, M.; Jayakumar, K. N.; Bharathi, P. Aryltitanium Species through the Reaction of *N*,*N*-Dialkylarylamines with TiCl4: Oxidative Coupling, N-Dealkylation, and Reaction with Electrophiles. *J. Org. Chem.* **2000**, *65*, 3548−3550.

(35) Berardi, F.; Ferorelli, S.; Colabufo, N. A.; Leopoldo, M.; Perrone, R.; Tortorella, V. A multireceptorial binding reinvestigation on an extended class of s ligands: N-[w-(indan-1-yl and tetralin-1-yl)alkyl] derivatives of 3,3-dimethylpiperidine reveal high affinities towards s1 and EBP sites. *Bioorg. Med. Chem.* **2001**, *9*, 1325−1335.

(36) Olsen, S. R.; Uhler, M. D. Affinity purification of the C-alpha and C-beta isoforms of the catalytic subunit of cAMP-dependent protein-kinase. *J. Biol. Chem.* **1989**, *264*, 18662−18666.

(37) Bailey, S. The CCP4 suite − programs for protein crystallography. *Acta Crystallogr. Sect. D: Biol. Crystallogr.* **1994**, *50*, 760−763.

(38) Potterton, E.; Briggs, P.; Turkenburg, M.; Dodson, E. A graphical user interface to the CCP4 program suite. *Acta Crystallogr. Sect. D: Biol. Crystallogr.* **2003**, *59*, 1131−1137.

(39) Gerber, P. R.; Muller, K. MAB, a generally applicable molecular-force field for structure modeling in medicinal chemistry. *J. Comput.-Aided Mol. Des.* **1995**, *9*, 251−268.

(40) Kraulis, P. J. MOLSCRIPT − a program to produce both detailed and schematic plots of protein structures. *J. Appl. Crystallogr.* **1991**, *24*, 946−950.

(41) Esnouf, R. M. Further additions to MolScript version 1.4, including reading and contouring of electron-density maps. *Acta Crystallogr. Sect. D: Biol. Crystallogr.* **1999**, *55*, 938−940.

(42) Merritt, E. A.; Bacon, D. J. Raster3D: Photorealistic molecular graphics. *Macromol. Crystallogr. B* 1997; pp 505−524.

JM049701N